Proceedings of IMECE2005
2005 ASME International Mechanical Engineering Congress and Exposition
November 5-11, 2005, Orlando, Florida USA

IMECE2005-82742

AN IMPLICIT MODEL FOR SNAKE ROBOT LOCOMOTION AND GAIT OPTIMIZATION

Appa Rao Nirakh
Department of Aerospace Engineering
The Pennsylvania State University
229 Hammond
University Park, Pennsylvania, 16802, U.S.A.

Sean N. Brennan
Department of Mechanical Engineering
The Pennsylvania State University
318 Leonhard
University Park, Pennsylvania, 16802, U.S.A.
sbrennan@psu.edu (Ph: 814-863-2430)

Farhan S. Gandhi
Department of Aerospace Engineering
The Pennsylvania State University
231C Hammond
University Park, Pennsylvania, 16802, U.S.A.
fgandhi@psu.edu (Ph: 814-865-1164)

ABSTRACT

The present study aims to develop dynamic models suitable for the analysis and design of robotic snakes. Specifically, this research presents an implicit model with a high degree of design flexibility, namely the ability to change the number of links and to vary friction in the model formulation. The implicit model is validated numerically by comparison to an explicit model with small number of links. The validated implicit model is then used to establish the optimal gait for a six-link snake robot to achieve locomotion with minimal power consumption. An iterative search is conducted over a range of operational parameters - amplitude of angular displacement inputs at each joint, relative phase lag between the sinusoidal displacement inputs at the joints, and frequency of sine-wave input - to determine the optimally efficient gait. Results indicate that, for a particular forward velocity, an optimal gait exists that minimizes power consumption. This optimal solution is validated experimentally via tests performed on a six-link snake robot.

KEYWORDS

Snake-robot; serpentine locomotion; optimal gait; hyper-redundant; mobile robot dynamics.

INTRODUCTION

Many researchers [1-11] have provided insight into the mathematical modeling of the kinematics and dynamics of serpentine locomotion. However, issues remain with these models, including questions about the level of mathematical complexity, little if any validation against experimental results, differing assumptions regarding robot/ground interaction, and limited analysis of power consumption as a function of gait parameters, operating speed.

Hirose [12-15] was the first to analyze snake-like locomotion by performing a series of experiments on actual snakes. These experiments sought to determine the path followed by a snake as it locomotes forward in the serpentine gait, referred to by Hirose as a Serpenoid Curve. Hirose also established that a net forward motion could be generated by applying time-varying torque along the length of the snake. Based on these results, a wheel-based, rigid-link snake-like locomotor was built capable of moving forward using applied joint torques without driving the wheels. However, the study was purely focused on the kinematics of motion, leaving open issues related to power consumption and practical determination of gait.

The Robotics group at the California Institute of Technology developed theory and mathematical models [16-19] to expand the study of the kinematics of snakes to include the dynamics of wheel-based snake-like locomotion. In these models, forward motion is generated by coupling internal shape changes with external holonomic constraints assuming no-slip constraints along the wheel axes. Qualitative experiments were conducted on a 30 degree-of-freedom hyper-redundant robot that demonstrated locomotion and other applications related to grasping, obstacle avoidance etc. However, there were few quantitative studies confirming the accuracy and results obtained by the mathematical models. Further, the predicted

locomotion was not studied with regard to minimizing power consumption.

Iwasaki [9] and his colleagues recently investigated robotic snake gaits that achieve forward locomotion at a prescribed speed while requiring the least power. Their mathematical model assumed a multi-link robotic snake without wheels. However, this model was not validated experimentally to confirm the optimal gait parameters established via analytical results.

The present study aims to develop dynamic models suitable for the analysis, design and control of robotic snakes. Specifically, this research seeks to develop an easily modifiable model which has flexibility with respect to number of links as well as the ability to change the friction model. The objectives of the present study are three fold:

- To provide a basic framework that allows study of the dynamics of planar serpentine locomotion of a discrete robotic snake model.
- To determine the operational parameters which optimize the gait of a six-link articulated snake robot to achieve minimum power consumption for a desired speed of locomotion.
- To experimentally validate the velocity-frequency relationship established via the mathematical analysis.

In this paper, mathematical modeling and analysis of the dynamics of a three-link articulated snake model is first described using two different methods: 1) a closed-form solution approach hereafter referred to as the explicit formulation and 2) an approach where link-to-link joint forces at a present time step are approximated using prior trajectories, an approach hereafter referred to as an implicit formulation. The next section presents a comparison of the two proposed methods. In the following section, the issue of optimal gait resulting in minimal power consumption at a given forward speed is studied. Simulation results for the optimally efficient motion are then provided. Finally, experimental results are presented to validate the analytical model. A Conclusions section summarizes the main results of the study.

MODELING AND ANALYSIS

For a snake robot, the key to generating forward locomotion is to exploit the difference in friction coefficients in the normal and tangential directions to the snake at the link-to-ground contact points. As convention, the normal direction is perpendicular to the link and the tangential direction is along the length of the link. Most of the studies [1, 5, 9, 12-15] assume the normal friction coefficient to be much larger than the tangential friction coefficient; with some [18, 19] assuming that slip in the lateral direction is negligible.

Analytical models of a general robotic snake usually consist of n rigid links actuated at the (n–1) joints connecting these links. Each link is generally assumed to have one point of contact with the ground at its center of gravity, an assumption also made in the present study. Additionally, the following assumptions are made within this study to derive the equations of motion of a snake robot:

- Each link has uniform mass distribution and the parameters for each link - length, mass etc. - are identical for all the links.
- A viscous friction model is employed to describe link-to-ground interaction (unless otherwise stated). The friction coefficients in the normal and tangential direction are assumed constant over the entire snake. Viscous friction is governed by: $F_{visc} = c \cdot v$; where v is the velocity in a particular direction, c, the viscous friction coefficient in that direction, and F_{visc}, the friction induced force at the point of contact in the direction of the velocity, v.
- Only planar serpentine locomotion is considered.

The general robotic snake system consists of a total of n+2 degrees of freedom with two degrees of freedom representing the planar position of the center of mass of the first link and the remaining degrees of freedom representing the orientations of the n links in the global reference frame.

To illustrate the mathematical formulation of an explicit model, a three-link model is considered as it is the simplest rigid-link snake robot that can locomote. The 5 independent degrees of freedom for a three-link model, are- $x, y, \theta_1, \theta_2, \theta_3$. A schematic of the model is shown in Fig. 1 and the free-body diagram of each link is shown in Fig. 2. The force and moment equilibrium equations: $\sum F_{x,i} = m_i \ddot{x}_i$, $\sum F_{y,i} = m_i \ddot{y}_i$ and $\sum M_{z,i} = I_i \ddot{\theta}_i$ for each of the three links can be written as follows:

Link 1:

$$F_{g,1}{}^{x} + F_{1x} = m\ddot{x}_1 \tag{1}$$

$$F_{g,1}{}^{y} + F_{1y} = m\ddot{y}_1 \tag{2}$$

$$T_1 - F_{1x} l \sin\theta_1 + F_{1y} l \cos\theta_1 = I_c \ddot{\theta}_1 \tag{3}$$

Link 2:

$$-F_{1x} + F_{g,2}{}^{x} + F_{2x} = m\ddot{x}_2 \tag{4}$$

$$-F_{1y} + F_{g,2}{}^{y} + F_{2y} = m\ddot{y}_2 \tag{5}$$

$$(T_2 - T_1) - (F_{1x} + F_{2x}) l \sin\theta_2 + (F_{1y} + F_{2y}) l \cos\theta_2 = I_c \ddot{\theta}_2 \tag{6}$$

Link 3:

$$-F_{2x} + F_{g,3}{}^{x} = m\ddot{x}_3 \tag{7}$$

$$-F_{2y} + F_{g,3}{}^{y} = m\ddot{y}_3 \tag{8}$$

$$-T_2 - F_{2x} l \sin\theta_3 + F_{2y} l \cos\theta_3 = I_c \ddot{\theta}_3 \tag{9}$$

where the parameters are defined as follows:

m	Mass of each link
l	Distance from the center of gravity of the link to the joint, equal to half of the link length, assuming uniform mass distribution
I_c	Mass moment of inertia of the link about the center of mass
x_i, y_i, θ_i	The global position and orientation of the i^{th} link
T_i	Torque applied at the i^{th} joint (between i^{th} and $(i+1)^{th}$ links)
$F_{g,i}{}^{x}, F_{g,i}{}^{y}$	Frictional forces between the i^{th} link and the ground at the center of gravity in the global coordinate system, resolved in the x and y directions.

F_{ix}, F_{iy} The joint forces between i^{th} and $(i+1)^{th}$ links in the global coordinate system, resolved in the x and y directions

Explicit Formulation for a three-link robotic snake

To obtain the time-varying positions and orientations of the various links, the Eqs. (1-9) have to be solved simultaneously. Two solution methods, namely explicit and implicit, are considered in this study. The explicit method utilizes the exact model without any approximations. The force and moment dynamic equations are simplified by rearranging them to eliminate the joint forces. These equations are further simplified by enforcing the compatibility conditions that describe the positions of all the links in terms of the five independent variables $x, y, \theta_1, \theta_2, \theta_3$. The resulting number of governing equations is always equal to the number of independent degrees of freedom; hence this solution method is hereafter referred to as an explicit method.

The challenge with the explicit model formulation is that the joint force and compatibility algebraic equations are highly nonlinear, making it difficult to write the governing differential equations in only the independent variables. One can overcome this algebraic difficulty by allowing more system differential equations than are necessary, e.g. by approximating the joint connections by spring-damper systems. The dynamics of the system are simulated individually for each link without the necessity of algebraic solutions for the joint forces. Further, the algebraic compatibility conditions are also not needed in the solution method. Because there are more equations than the number of independent degrees of freedom, this solution method is hereafter referred to as an implicit method. These distinctions between explicit and implicit formulations are best illustrated by direct comparison, presented in the following sections.

As an illustration, the explicit equations of motion for a three-link snake are now derived. From Fig. 1, the coordinates of the center of mass of each link can be expressed as a function of the aforementioned five independent variables, $x, y, \theta_1, \theta_2, \theta_3$, as follows:

$$x_1 = x \tag{10}$$

$$y_1 = y \tag{11}$$

$$x_2 = x + l\cdot\cos\theta_1 + l\cdot\cos\theta_2 \tag{12}$$

$$y_2 = y + l\cdot\sin\theta_1 + l\cdot\sin\theta_2 \tag{13}$$

$$x_3 = x + l\cdot\cos\theta_1 + 2l\cdot\cos\theta_2 + l\cdot\cos\theta_3 \tag{14}$$

$$y_3 = y + l\cdot\sin\theta_1 + 2l\cdot\sin\theta_2 + l\cdot\sin\theta_3 \tag{15}$$

Differentiating Eqs. (10-15) with respect to time yields the velocities of the center of mass of the links in the global coordinate system as:

$$\dot{x}_1 = \dot{x} \tag{16}$$

$$\dot{y}_1 = \dot{y} \tag{17}$$

$$\dot{x}_2 = \dot{x} - l\dot{\theta}_1\sin\theta_1 - l\dot{\theta}_2\sin\theta_2 \tag{18}$$

$$\dot{y}_2 = \dot{y} + l\dot{\theta}_1\cos\theta_1 + l\dot{\theta}_2\cos\theta_2 \tag{19}$$

$$\dot{x}_3 = \dot{x} - l\dot{\theta}_1\sin\theta_1 - 2l\dot{\theta}_2\sin\theta_2 - l\dot{\theta}_3\sin\theta_3 \tag{20}$$

$$\dot{y}_3 = \dot{y} + l\dot{\theta}_1\cos\theta_1 + 2l\dot{\theta}_2\cos\theta_2 + l\dot{\theta}_3\cos\theta_3 \tag{21}$$

Similarly, differentiating the velocities i.e. Eqs. (16-21) with respect to time yields the accelerations of the center of mass of the links as:

$$\ddot{x}_1 = \ddot{x} \tag{22}$$

$$\ddot{y}_1 = \ddot{y} \tag{23}$$

$$\ddot{x}_2 = \ddot{x} - l\ddot{\theta}_1\sin\theta_1 - l\ddot{\theta}_2\sin\theta_2 - l\dot{\theta}_1^{\,2}\cos\theta_1 - l\dot{\theta}_2^{\,2}\cos\theta_2 \tag{24}$$

$$\ddot{y}_2 = \ddot{y} + l\ddot{\theta}_1\cos\theta_1 + l\ddot{\theta}_2\cos\theta_2 - l\dot{\theta}_1^{\,2}\sin\theta_1 - l\dot{\theta}_2^{\,2}\sin\theta_2 \tag{25}$$

$$\ddot{x}_3 = \ddot{x} - l\ddot{\theta}_1\sin\theta_1 - 2l\ddot{\theta}_2\sin\theta_2 - l\ddot{\theta}_3\sin\theta_3 - l\dot{\theta}_1^{\,2}\cos\theta_1 - 2l\dot{\theta}_2^{\,2}\cos\theta_2 - l\dot{\theta}_3^{\,2}\cos\theta_3 \tag{26}$$

$$\ddot{y}_3 = \ddot{y} + l\ddot{\theta}_1\cos\theta_1 + 2l\ddot{\theta}_2\cos\theta_2 + l\ddot{\theta}_3\cos\theta_3 - l\dot{\theta}_1^{\,2}\sin\theta_1 - 2l\dot{\theta}_2^{\,2}\sin\theta_2 - l\dot{\theta}_3^{\,2}\sin\theta_3 \tag{27}$$

The contact forces between the ground and the link at the center of mass are modeled assuming the viscous friction model stated previously. The friction coefficients and hence the contact forces are defined locally, i.e. in the normal and tangential directions and then transformed back into the global coordinate system. From Fig. 3, the contact forces in the tangential and normal directions can be written as:

$$F_{g,i}^{\ t} = C_i^{\ t}\cdot v_i^{\ t} = C_i^{\ t}\cdot(\dot{x}_i\cos\theta_i + \dot{y}_i\sin\theta_i) \tag{28}$$

$$F_{g,i}^{\ n} = C_i^{\ n}\cdot v_i^{\ n} = C_i^{\ n}\cdot(-\dot{x}_i\sin\theta_i + \dot{y}_i\cos\theta_i) \tag{29}$$

Equations (28-29) can be expressed in matrix form as follows:

$$\begin{Bmatrix} F_{g,i}^{\ t} \\ F_{g,i}^{\ n} \end{Bmatrix} = \begin{bmatrix} C_i^{\ t} & 0 \\ 0 & C_i^{\ n} \end{bmatrix}\cdot\begin{bmatrix} \cos\theta_i & \sin\theta_i \\ -\sin\theta_i & \cos\theta_i \end{bmatrix}\cdot\begin{Bmatrix} \dot{x}_i \\ \dot{y}_i \end{Bmatrix} \tag{30}$$

The contact forces in the normal and tangential directions can be transformed back into the global coordinate system as follows:

$$F_{g,i}^{\ x} = F_{g,i}^{\ t}\cos\theta_i - F_{g,i}^{\ n}\sin\theta_i \tag{31}$$

$$F_{g,i}^{\ y} = F_{g,i}^{\ t}\sin\theta_i + F_{g,i}^{\ n}\cos\theta_i \tag{32}$$

Using Eqs. (30-32) the friction forces associated with the i^{th} link can be expressed in the global coordinate system as:

$$\begin{Bmatrix} F_{g,i}^{\ x} \\ F_{g,i}^{\ y} \end{Bmatrix} = \begin{bmatrix} \cos\theta_i & -\sin\theta_i \\ \sin\theta_i & \cos\theta_i \end{bmatrix}\cdot\begin{bmatrix} C_i^{\ t} & 0 \\ 0 & C_i^{\ n} \end{bmatrix}\cdot\begin{bmatrix} \cos\theta_i & \sin\theta_i \\ -\sin\theta_i & \cos\theta_i \end{bmatrix}\cdot\begin{Bmatrix} \dot{x}_i \\ \dot{y}_i \end{Bmatrix} \tag{33}$$

Equations (10-33) describe how the compatibility constraints and frictional forces enter the dynamic model. It is now possible to write the governing differential equations, with the first goal to eliminate joint forces. One can eliminate several coupling forces by summing Eqs. (1), (4), and (7):

$$m\left(\ddot{x}_1 + \ddot{x}_2 + \ddot{x}_3\right) = F_{g,1}{}^x + F_{g,2}{}^x + F_{g,3}{}^x \tag{34}$$

Similarly, summing Eqs. (2), (5), and (8) results in:

$$m\left(\ddot{y}_1 + \ddot{y}_2 + \ddot{y}_3\right) = F_{g,1}{}^y + F_{g,2}{}^y + F_{g,3}{}^y \tag{35}$$

The joint forces, F_{ix} and F_{iy}, are to be eliminated from Eqs. (3), (6) and (9) to obtain the remaining governing equations. This is achieved by expressing the joint forces in terms of known quantities. Summing Eqs. (4), (7) and (5), (8) and solving for F_{1x} and F_{1y} respectively results in:

$$-F_{1x} = m\left(\ddot{x}_2 + \ddot{x}_3\right) - \left(F_{g,2}{}^x + F_{g,3}{}^x\right) \tag{36}$$

$$-F_{1y} = m\left(\ddot{y}_2 + \ddot{y}_3\right) - \left(F_{g,2}{}^y + F_{g,3}{}^y\right) \tag{37}$$

Solving Eqs. (7) and (8) for F_{2x} and F_{2y} yields:

$$-F_{2x} = m\ddot{x}_3 - F_{g,3}{}^x \tag{38}$$

$$-F_{2y} = m\ddot{y}_3 - F_{g,3}{}^y \tag{39}$$

The right hand side of Eqs. (34) and (35) can be expressed solely in terms of the independent variables using the generalized Eq. (33) and Eqs. (16-21). The resulting differential equations are functions of linear and angular displacements and velocities of the center of mass of the links. The left hand side of Eqs. (34) and (35) can be rewritten in terms of the independent variables and their derivatives alone using Eqs. (22-27). These equations, upon simplification, yield:

$$\begin{aligned} &3m\ddot{x} - ml\left(2\ddot{\theta}_1 \sin\theta_1 + 3\ddot{\theta}_2 \sin\theta_2 + \ddot{\theta}_3 \sin\theta_3\right) \\ &= Q_1 + ml\left(2\dot{\theta}_1{}^2 \cos\theta_1 + 3\dot{\theta}_2{}^2 \cos\theta_2 + \dot{\theta}_3{}^2 \cos\theta_3\right) \end{aligned} \tag{40}$$

$$\begin{aligned} &3m\ddot{y} + ml\left(2\ddot{\theta}_1 \cos\theta_1 + 3\ddot{\theta}_2 \cos\theta_2 + \ddot{\theta}_3 \cos\theta_3\right) \\ &= Q_2 + ml\left(2\dot{\theta}_1{}^2 \sin\theta_1 + 3\dot{\theta}_2{}^2 \sin\theta_2 + \dot{\theta}_3{}^2 \sin\theta_3\right) \end{aligned} \tag{41}$$

where, Q_1 and Q_2 are defined as:

$$Q_1 = F_{g,1}{}^x + F_{g,2}{}^x + F_{g,3}{}^x \tag{42}$$

$$Q_2 = F_{g,1}{}^y + F_{g,2}{}^y + F_{g,3}{}^y \tag{43}$$

Substituting Eqs. (36-37) into Eq. (3) and simultaneously using Eqs. (22-27) and simplifying results in:

$$\begin{aligned} &I_{01}\ddot{\theta}_1 + 2ml\left(\ddot{y}\cos\theta_1 - \ddot{x}\sin\theta_1\right) \\ &+ ml^2\left[3\ddot{\theta}_2 \cos\left(\theta_1 - \theta_2\right) + \ddot{\theta}_3 \cos\left(\theta_3 - \theta_1\right)\right] \\ &= T_1 + Q_3 + ml^2\left\{-3\dot{\theta}_2{}^2 \sin\left(\theta_1 - \theta_2\right) + \dot{\theta}_3{}^2 \sin\left(\theta_3 - \theta_1\right)\right\} \end{aligned} \tag{44}$$

where, I_{01} and Q_3 is defined as:

$$\begin{aligned} I_{01} &= I_c + 2ml^2 \\ Q_3 &= -\left(F_{g,2}{}^x + F_{g,3}{}^x\right) l \sin\theta_1 + \left(F_{g,2}{}^y + F_{g,3}{}^y\right) l \cos\theta_1 \end{aligned} \tag{45}$$

Similarly, using Eqs. (36-39) in Eq. (6) and simplifying utilizing Eqs. (22-27) yields:

$$\begin{aligned} &I_{02}\ddot{\theta}_2 + 3ml\left(\ddot{y}\cos\theta_2 - \ddot{x}\sin\theta_2\right) \\ &+ ml^2\left[3\ddot{\theta}_1 \cos\left(\theta_1 - \theta_2\right) + 2\ddot{\theta}_3 \cos\left(\theta_2 - \theta_3\right)\right] \\ &= \left(T_2 - T_1\right) + Q_4 + ml^2\left\{3\dot{\theta}_1^2 \sin\left(\theta_1 - \theta_2\right) - 2\dot{\theta}_3^2 \sin\left(\theta_2 - \theta_3\right)\right\} \end{aligned} \tag{46}$$

where, I_{02} and Q_4 is defined as:

$$\begin{aligned} I_{02} &= I_c + 5ml^2 \\ Q_4 &= -\left(F_{g,2}{}^x + 2F_{g,3}{}^x\right) l \sin\theta_2 + \left(F_{g,2}{}^y + 2F_{g,3}{}^y\right) l \cos\theta_2 \end{aligned} \tag{47}$$

Finally, using Eqs. (22-27) and Eqs. (38, 39) in Eq. (9) and simplifying yields the last of the five governing equations as:

$$\begin{aligned} &I_{03}\ddot{\theta}_3 + ml\left(\ddot{y}\cos\theta_3 - \ddot{x}\sin\theta_3\right) \\ &+ ml^2\left[\ddot{\theta}_1 \cos\left(\theta_3 - \theta_1\right) + 2\ddot{\theta}_2 \cos\left(\theta_2 - \theta_3\right)\right] \\ &= \left(-T_2\right) + Q_5 + ml^2\left\{-\dot{\theta}_1^2 \sin\left(\theta_3 - \theta_1\right) + 2\dot{\theta}_2^2 \sin\left(\theta_2 - \theta_3\right)\right\} \end{aligned} \tag{48}$$

Where, I_{03} and Q_5 is defined as:

$$\begin{aligned} I_{03} &= I_c + ml^2 \\ Q_5 &= -F_{g,3}{}^x l \sin\theta_3 + F_{g,3}{}^y l \cos\theta_3 \end{aligned} \tag{49}$$

Equations (40, 41, 44, 46, and 48) are the five equations governing the dynamics of a three-link articulated robot. Rewriting these equations in matrix form yields:

$$\begin{bmatrix} 3m & 0 & -2ml\sin\theta_1 & -3ml\sin\theta_2 & -ml\sin\theta_3 \\ 0 & 3m & 2ml\cos\theta_1 & 3ml\cos\theta_2 & ml\cos\theta_3 \\ -2ml\sin\theta_1 & 2ml\cos\theta_1 & I_{01} & 3ml^2\cos(\theta_1-\theta_2) & ml^2\cos(\theta_3-\theta_1) \\ -3ml\sin\theta_2 & 3ml\cos\theta_2 & 3ml^2\cos(\theta_1-\theta_2) & I_{02} & 2ml^2\cos(\theta_2-\theta_3) \\ -ml\sin\theta_3 & ml\cos\theta_3 & ml^2\cos(\theta_3-\theta_1) & 2ml^2\cos(\theta_2-\theta_3) & I_{03} \end{bmatrix}$$

$$\times \begin{Bmatrix} \ddot{x} \\ \ddot{y} \\ \ddot{\theta}_1 \\ \ddot{\theta}_2 \\ \ddot{\theta}_3 \end{Bmatrix} = \begin{bmatrix} 0 \\ 0 \\ T_1 \\ T_2 - T_1 \\ -T_2 \end{bmatrix} + \begin{bmatrix} ml(2\dot{\theta}_1^2\cos\theta_1 + 3\dot{\theta}_2^2\cos\theta_2 + \dot{\theta}_3^2\cos\theta_3) \\ ml(2\dot{\theta}_1^2\sin\theta_1 + 3\dot{\theta}_2^2\sin\theta_2 + \dot{\theta}_3^2\sin\theta_3) \\ ml^2[-3\dot{\theta}_2^2\sin(\theta_1-\theta_2) + \dot{\theta}_3^2\sin(\theta_3-\theta_1)] \\ ml^2[3\dot{\theta}_1^2\sin(\theta_1-\theta_2) - 2\dot{\theta}_3^2\sin(\theta_2-\theta_3)] \\ ml^2[-\dot{\theta}_1^2\sin(\theta_3-\theta_1) + 2\dot{\theta}_2^2\sin(\theta_2-\theta_3)] \end{bmatrix} + \begin{bmatrix} Q_1 \\ Q_2 \\ Q_3 \\ Q_4 \\ Q_5 \end{bmatrix} \tag{50}$$

The above equation is of the form $A(X)\cdot\ddot{X} = f\left(X, \dot{X}\right)$ or $\ddot{X} = g\left(X, \dot{X}\right)$. These simplified equations can be solved numerically. In this study the MATLAB Simulink software is used to numerically integrate Eq. (50) to obtain a solution $X(t)$.

Solution methods describing the kinematics and dynamics of the serpentine locomotion resembling the above explicit method detailed have been presented in the literature by many researchers [1, 4, 5, 7-10, and 15-19]. Although each solution method differs slightly, they all share an ultimate goal of obtaining the time-varying positions and orientations of the links.

Implicit Formulation for a three-link robotic snake

While it is relatively easy to derive the explicit equations of motion for a three-link model, it is algebraically quite challenging and tedious to derive a similar set of equations for snakes with larger number of links. The implicit method simplifies the algebraic manipulations considerably by relaxing an algebraic constraint of connection between the joints and instead modeling them by spring-damper systems. The damper and spring are designed to have vibration dynamics several orders of magnitude faster than the snake's gross motion and therefore this motion should not greatly affect the predicted motion of the snake. This assumption is tested in later sections of this study.

Although replacing each joint's algebraic constraints with joint dynamics greatly increases the order of the dynamic model, it greatly simplifies the necessary mathematical manipulations. Specifically, the positions, velocities and accelerations of the center of mass of the links need not be expressed in terms of the position of the center of mass of the first link, orientations of the links, e.g. in $x, y, \theta_1, \theta_2, \theta_3$, and their derivatives. The original snake consisting of one articulated *n*-link body is therefore deconstructed into *n* coupled but independent bodies. The dynamics of the spring-damper system can be simulated to directly obtain the coupling forces between joints while simultaneously solving for the dynamics of the collective robot snake system. Thus, this method does not require solving for the joint forces as in the explicit method.

The primary disadvantage of the implicit method over the explicit is that the additional differential equations greatly increase the required simulation time. With the steady and exponential increase in desktop computing capability, this tradeoff is increasingly unimportant.

To model the joint connections by spring-damper systems, the spring stiffness and damping constant need to be chosen. The spring stiffness is chosen such that the joints are stiff enough to exhibit very fast dynamics and damping constant is chosen to have as minimal vibration as possible. All locomotion torques at each joint are assumed to span the joint such that an equal and opposite torque acts on each link. From Fig. 4, the expressions for the joint forces at i^{th} joint can be written as:

$$F_{ix} = k_i \cdot \left(x^i{}_r - x^i{}_l\right) + c_i \cdot \left(\dot{x}^i{}_r - \dot{x}^i{}_l\right) \tag{51}$$

$$F_{iy} = k_i \cdot \left(y^i{}_r - y^i{}_l\right) + c_i \cdot \left(\dot{y}^i{}_r - \dot{y}^i{}_l\right) \tag{52}$$

where the parameters are defined as follows:

k_i Spring stiffness.

c_i Damping constant.

$x^i{}_r, y^i{}_r$ Coordinates of the i^{th} joint expressed as a function of the coordinates of the center of mass of the link to the right of the joint, i.e. $(i+1)^{th}$ link.

$x^i{}_l, y^i{}_l$ Coordinates of the i^{th} joint expressed as a function of the coordinates of the center of mass of the link to the left of the joint, i.e. i^{th} link.

The coordinates $x^i{}_l$, $y^i{}_l$, $x^i{}_r$, and $y^i{}_r$ can be expressed in terms of the coordinates of the centers of mass of i^{th} and $(i+1)^{th}$ links, (x_i, y_i) and (x_{i+1}, y_{i+1}) respectively as:

$$x^i{}_r = x_{i+1} - l \cdot \cos\theta_{i+1} \tag{53}$$

$$x^i{}_l = x_i + l \cdot \cos\theta_i \tag{54}$$

$$y^i{}_r = y_{i+1} - l \cdot \sin\theta_{i+1} \tag{55}$$

$$y^i{}_l = y_i + l \cdot \sin\theta_i \tag{56}$$

The time derivatives of the positions, i.e. $\dot{x}^i{}_l$, $\dot{y}^i{}_l$, $\dot{x}^i{}_r$, and $\dot{y}^i{}_r$ are obtained by differentiating Eqs. (53-56), which are obtained numerically using velocities from the previous time steps. Besides Eqs. (51-56), the friction formulation equations are also needed, i.e. Eqs. (28-33) as established in the explicit formulation section.

With the joint and contact forces known, the implicit method is easily solved numerically. Eqs. (1-9) are integrated using the MATLAB Simulink software to determine the positions and velocities of the center of mass of each link. A flowchart describing the implementation of implicit model in Simulink is presented in Fig. 5.

COMPARISON OF IMPLICIT AND EXPLICIT FORMULATION RESULTS

To confirm that the implicit and explicit formulations are mathematically equivalent, the dynamics of a three-link snake model are simulated using both methods. The relative errors in the rotations and velocities are compared. Relative error in rotation is defined as $\Delta\theta(t) = \theta_{im}(t) - \theta_{ex}(t)$, where θ_{im} and θ_{ex} are the rotations calculated by the implicit and explicit methods respectively. The relative errors in other quantities are calculated similarly. The time-step used for the simulations is 0.001 s. Further reduction in time step resulted in only a maximum of 0.1% change in the calculated displacement and velocity values.

Figures 6 and 7 represent the relative errors between the implicit and explicit rotation and translational velocities of the tail link, i.e. link 1 for a three-link snake robot. The amplitude of motion considered is 30 deg, the relative phase lag is 90 deg, and the frequency of sine-wave input is 3 rad/s. It appears from these plots that the magnitude of the relative error between the two models is of the order of 10^{-3}, which is quite small as compared to the amplitude of motion ($\pi/6$). Similar plots are obtained for the other two links. Such results suggest very close agreement between the two methods.

OPTIMALLY EFFICIENT SERPENTINE LOCOMOTION

Having confirmed that the implicit method predicts locomotion behavior as well as an explicit model for a simple three-link robot, the implicit model is now used to analyze a six-link robot. Specifically, locomotion dynamics are studied to determine the optimal gait that gives locomotion with minimal power consumption at a given forward velocity. Prior studies [9, 15] indicate that the undulatory motion of snake can be replicated by sending a traveling sine wave along the length of the snake and that dynamics of the snake using joint inputs as a specified angle versus torque are related by a decoupling. This wave can be approximated in a discrete snake model by incrementing the phase angle of an applied sinusoidal torque or the prescribed angular motion at each joint of the snake robot. This analysis considers the input to be a commanded joint angle with the angular motion at i^{th} joint described by the form:

$$\theta_i(t) = \alpha \sin(\omega t + \beta_i) \tag{57}$$

where, $\beta_i = (i-1)\beta$ and $i = 1, 2, \ldots n-1$.

The parameter ω (frequency of commanded angular motion) is related to the speed of locomotion, while the parameters α (amplitude of sinusoidal input) and β (phase lag) are related to the shape of forward motion. The optimally efficient motion is defined by [9] as the set of parameters, α, β and ω that result in the least mean power consumption for a desired mean forward velocity. The mean power input is determined by averaging the periodic input power over 15 cycles, or equivalently over a time period of $15 \cdot \frac{2\pi}{\omega}$ s after the snake has achieved steady-state locomotion. The mean forward velocity is the time averaged velocity of the center of mass of the entire snake in the global x-direction over 15 cycles. Other design parameters also affect the optimal motion; these include the tangential and normal friction coefficients, the mass and length of the link, and the number of links. But these other parameters are fixed in the design and operating environment of the snake and cannot be modified by the input to the joints, e.g. the snake's control algorithm.

To determine the optimally efficient gait, this study uses an iterative search through a range of the parameters α, β, and ω. When a grid point was found to be locally optimal, a linear optimization algorithm was used to further refine the parameter estimate such that the numerical estimate of the optimal parameters is not limited to the coarse grid spacing. Some parameters remain constant over the entire analysis: mass of the link, m (1 kg), length of the link, l (6 cm), tangential friction coefficient, C_t (0.1 N-s.m^{-1}), normal friction coefficient, C_n (10 N-s.m^{-1}) and the number of links, n (6). The parameter space over which the iterative search is performed is: ω (rads^{-1}) = 1.0, 2.0, 3.0,..., 20.0, α (deg) = 5, 10, 15,..., 75 and β (deg) = 20, 25, 30,..., 90. The other simulation parameters used are: $c_i = 1$ N-s/m, $k_i = 1000$ N/m. and a fixed time step of 0.001 s. Discussion regarding the results generated by the simulations is presented in the following section.

RESULTS AND DISCUSSION

Figure 8 shows the variation of the mean power input (P_{in}) versus the desired mean forward velocity (V_{des}). It can be seen from the figure (solid line joining the optimal points) that an optimal solution does indeed exist for a given desired locomotion velocity. The variations of the optimal parameters: frequency (ω), phase (β) and amplitude (α) with the desired mean velocity are plotted in Figs. 9–11. The optimal frequency ω_{opt} appears to vary almost linearly with the desired velocity. The optimal phase β_{opt} and optimal amplitude α_{opt} appear to be nearly constant at 80 deg and 30 deg respectively, independent of the desired velocity. A trace of the path followed by the snake robot at α = 30 deg, β = 80 deg and ω = 5 rad/s is presented in Fig. 12 and a plot of the snake's position and orientation at six instances over one time period is shown in Fig. 13.

Compared to an earlier study [9], the results of the present research match qualitatively but not quantitatively. For instance, the present study predicts that an optimal motion should consist of slightly more than one full sine wave (1.3 sine waves), while this earlier study predicted optimal motion for exactly one sine wave. This is equivalently described by comparing the optimal phase, β_{opt} of a six-link robot. The present study predicts β_{opt} to be at approximately 80 deg between links, while [9] predicts this to be at 60 deg. The variation of optimal amplitude α_{opt} predicted by [9] seems to be roughly linear with desired velocity, while the present study predicts a nearly constant value at 30 deg. The optimal frequency of serpentine motion, ω_{opt}, is predicted by the present study to vary linearly with V_{des} in agreement with this prior work [9].

EXPERIMENTAL VALIDATION

To validate the analytical results, a snake robot which consists of six rigid wheeled members actuated by servos at the five joints is built. The wheels are chosen so that they have little slip in the lateral direction i.e. they are able to generate large friction coefficients in the normal direction and have relatively low friction coefficients in the tangential or forward direction. Thus the experimental conditions were designed to qualitatively match the assumed friction characteristics in the analytic formulation. A picture of the six link snake robot on treadmill is provided in Fig. 14. The mass of each link, m is 75.6 grams and the length of each link (2*l) is 7.6 cm. The friction characteristics are measured by utilizing the capability of the treadmill to tilt it to a desired angle of forward inclination (γ) and run at a desired velocity.

To measure the tangential friction characteristics, the snake is set free perfectly straight on the treadmill i.e. relative angles between the links to be 180 deg. Initially γ is set to a very small angle (2 deg in this case) and then increased steadily. The velocity of the treadmill is increased until the gravity of the snake almost balances the frictional forces on the snake. The above process is repeated in steps of 0.2 deg until a speed of 1 m/s is reached which is approximately the physical limit of the snake. Knowing the mass of the snake, m, and the inclination angle, γ, the tangential friction force, F_t can be calculated as:

$$F_t = m \cdot g \cdot \sin\gamma \tag{58}$$

where, g is the acceleration due to gravity

Figure 15 shows a plot of the tangential friction characteristics. Assuming the tangential friction force to vary linearly with the tangential velocity, the tangential friction characteristics are predicted as:

$$F_t = 0.084 \cdot v_t + 0.14 \tag{59}$$

where, v_t is the velocity in the tangential direction

To estimate the friction characteristics in the normal direction, the links are slightly bent alternately with the relative angle between adjacent links slightly less than 180 deg (165 deg in this case ($=180-2\lambda$)). The friction measurements are repeated as indicated above. The force equilibrium equation in the direction of treadmill velocity can be written as:

$$F_t \cdot \cos\lambda + F_n \cdot \sin\lambda = m \cdot g \cdot \sin\gamma \tag{60}$$

where, F_t is the friction force in the tangential direction and F_n is the friction force in the normal direction

Assuming F_t known in Eq. 60, solving for F_n yields:

$$F_n = \frac{\left(m \cdot g \cdot \sin\gamma - F_t \cdot \cos\lambda\right)}{\sin\lambda} \tag{61}$$

A plot of the normal friction characteristics is shown in Fig. 16. Again, assuming a linear variation, the normal friction characteristics are predicted as follows:

$$F_n = 1.2 \cdot v_n + 0.27 \tag{62}$$

where, v_n is the velocity in the normal direction

Equations (61) and (62) indicate that the friction characteristics of a snake operating on a treadmill surface resemble that of a viscous friction model with an offset or in other words, a Bingham friction model. The implicit method is then modified to account for this change in the friction model.

Tests are performed on the treadmill to validate the frequency-velocity relationship for a six-link snake robot at α = 70 deg and β = 75 deg. A plot of the variation of analytical and experimental velocities with frequency at this parameter setting is shown in Fig. 17. The analytical velocity seems to match closely with the experimentally measured velocity. The slight variation in the values predicted by the experiment can be attributed to the difficulty in estimating the friction characteristics of the snake in the normal direction. Normal friction characteristics are relatively more sensitive to minor variations in the angle λ, while the tangential friction characteristics are independent and these differences get amplified at higher frequencies.

CONCLUSIONS AND FUTURE WORK

An implicit method to study the dynamics of serpentine locomotion has been established. Using this implicit model, optimal gait of a six-link snake robot that results in minimal power consumption for a given forward velocity is established for a viscous friction model. Further, friction characteristics are determined experimentally for a six-link snake robot. The nature of frequency-velocity relationship at α = 70 deg and β = 75 deg is validated via experimental testing.

As future work, additional consideration will be given to the friction modeling, particularly with regard to establishing the optimal gait for the Bingham friction model. The large static friction measured in the tangential friction characteristic curve does not affect the locomotion significantly since the snake's motion is always enforced in the longitudinal direction. However, a combined static/viscous friction model will almost certainly impact predicted snake behavior. Additionally, methods to measure or estimate the robot/ground interaction to further improve adaptability to the environment and minimize power consumption will also be studied.

REFERENCES

[1] Shan, Y., and Koren, Y., 1993, "Design and Motion Planning of a Mechanical Snake," IEEE Trans. Sys. Man Cyb., **23**(4), pp 1091-1100.

[2] Worst, R., and Linnemann, R., 1996, "Construction and Operation of a Snake-Like Robot," Proc. of IEEE Int. Joint Symp. Intel. Sys., Gaithersburg, MD, pp 164-169.

[3] Dowling, K., 1997, Limbless Locomotion: Learning to Crawl with a Snake Robot," Ph.D. thesis, Carnegie Mellon University, Pittsburgh, PA.

[4] Klaassen, B., and Paap, K., 1999, "GMD-SNAKE2: A Snake-Like Robot Driven by Wheels and a Method for Motion Control," Detroit, MI, Proc. of IEEE Int. Conf. on Robotics and Auto., pp 3014-3019.

[5] Ma, S., 1999, "Analysis of Snake Movement Forms for Realization of Snake-like Robot," Proc. IEEE Int. conf. Robotics and Auto., Detroit, MI, pp 3007-3013.

[6] Dowling, K., 1999, "Limbless Locomotion: Learning to Crawl," Proc. IEEE Int. conf. Robotics and Auto., Detroit, MI,

[7] Spanos, P., Berka, R., and Tratskas, P., 2000, "Multisegment Large Space Robot: Concept and Design," J. Aerospace Eng., 13(4), pp 123-132.

[8] Liu, H., Yan, G., and Ding, G., 2001, "Research on the Locomotion Mechanism of Snake-like robot," Int. symp. On Micromechatronics and Human Science, pp 183-188.

[9] Saito, M., Fukaya, M., and Iwasaki, T., 2002, "Modeling, Analysis and Synthesis of Serpentine Locomotion with a Multilink Robotic Snake," IEEE Control Systems Magazine, **22**(1), pp.375-382.

[10] Nilsson, M., 2004, "Serpentine locomotion on surfaces with uniform friction," Sendal, Japan, Proc. of IEEE Int. conf. on Intel. Robots Sys., pp 1751 – 1755.

[11] Jalbert, J., Kashin, S., Ayers, J., 1995 "Design Considerations and Experiments on a Biologically-based Undulatory Lamprey-like AUV," Proc. Int. Symp. Unmanned Untethered Submersible Technology, Autonomous Undersea Systems Institute, Portsmouth, N.H., pp 124-138.

[12] Umetani, Y., and Hirose, S., 1974, "Biomechanical Study of Serpentine Locomotion," Udine, Italy, Proc. 1st RoManSy Symp., pp 171-184.

[13] Hirose, S., and Umetani, Y., 1976, "Kinematic Control of Active Cord Mechanism with Tactile Sensors," Proc. of 2nd Int. CISM-IFT Symp. On Theory and Practice of Robots and Manipulators, pp 241-252.

[14] Hirose, S., and Morishima, A., 1990, "Design and Control of a Mobile Robot with an Articulated Body," International J. of Robotics Research, 9(2), pp 289-298.

[15] Hirose, S., 1993, *Biologically Inspired Robots*, Oxford University Press, New York, NY.

[16] Chirikjian, G. S., and Burdick, J. W., 1991, "Kinematics of Hyper Redundant Locomotion with Applications to Grasping," IEEE Int. Conf. on Robotics and Automation, Sacramento, CA, pp 720-727.

[17] Burdick, J.W., and Radford, J., 1993, "A sidewinding Locomotion Gait for Hyper Redundant Robots," Atlanta, GA, IEEE Int. Conf. on Robotics and Automation, pp 101-106.

[18] Ostrowski, J.P., 1995, "The Mechanics and Control of Undulatory Robotic Locomotion," Ph.D. thesis, California Institute of Technology, Pasadena, CA.

[19] Ostrowski, J., and Burdick, J., 1998, "The Geometric Mechanics of Undulatory Robotic Locomotion," Int. J. Robotics Res., **120-D**(7), pp 683-701.

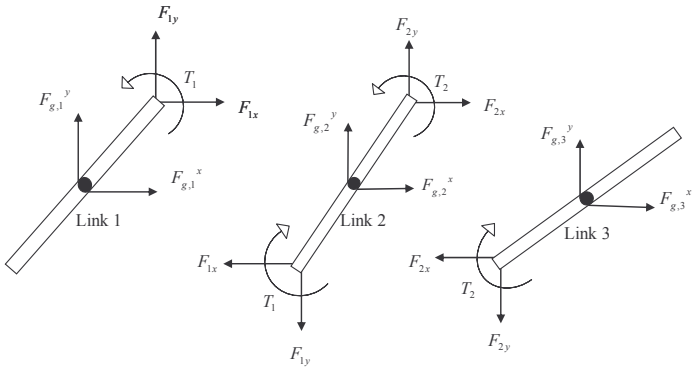

Fig. 2: Free-body Diagram of the three-link model

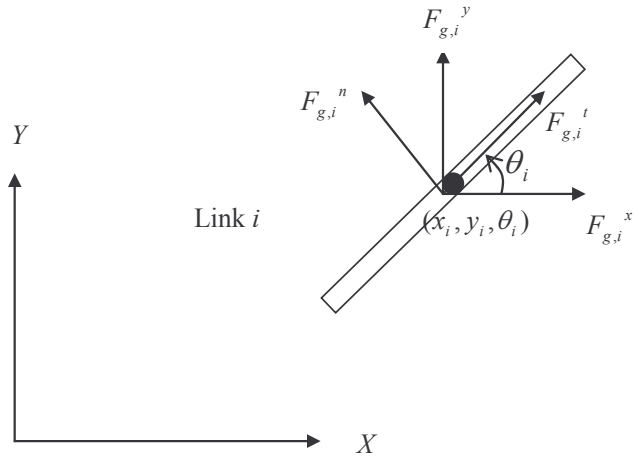

Fig. 3: Frictional forces on a generic link

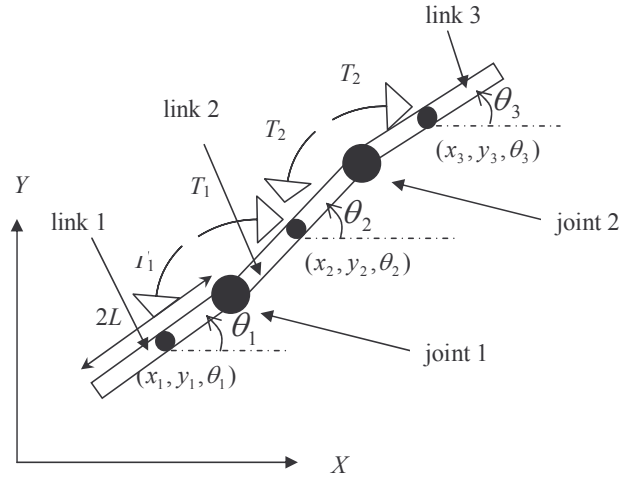

Fig. 1: Three-link articulated snake model

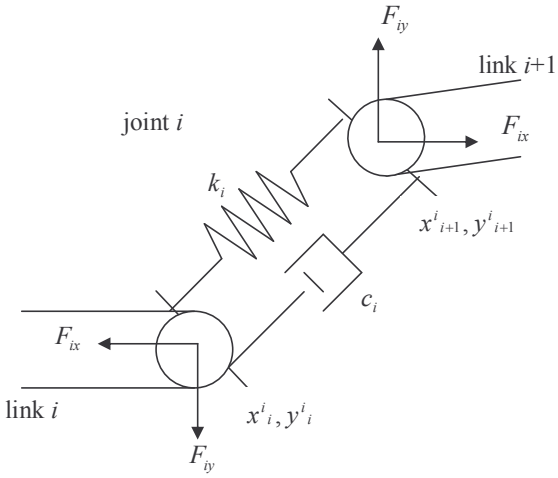

Fig. 4: Representation of spring-damper system at the i^{th} joint

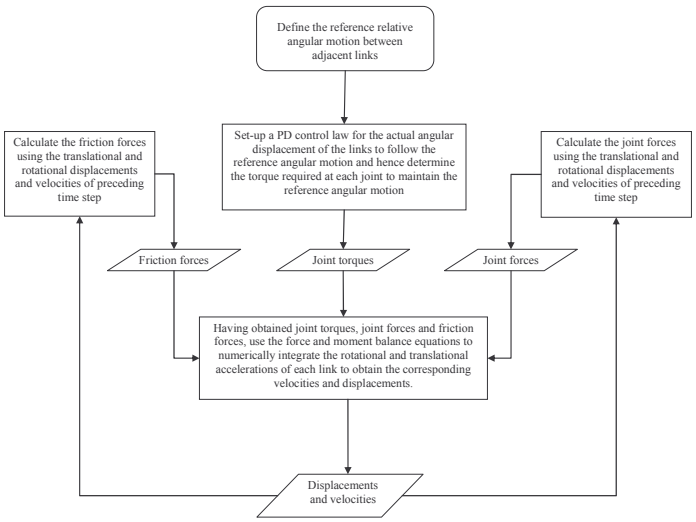

Fig. 5: Flowchart for the Simulink implementation of implicit formulation

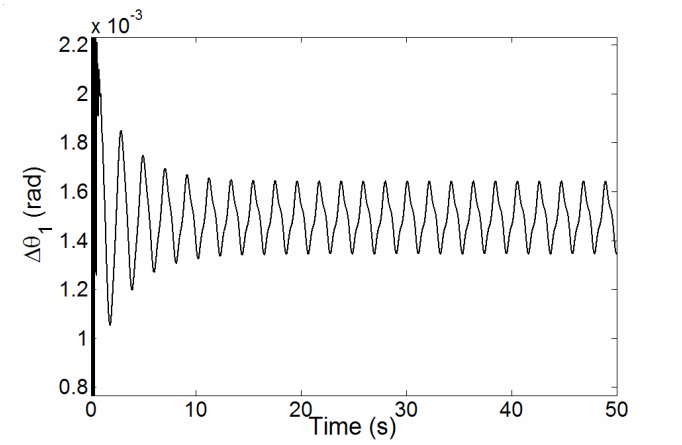

Fig. 6: Plot of the relative error in the angular displacement of the tail link of a three-link model

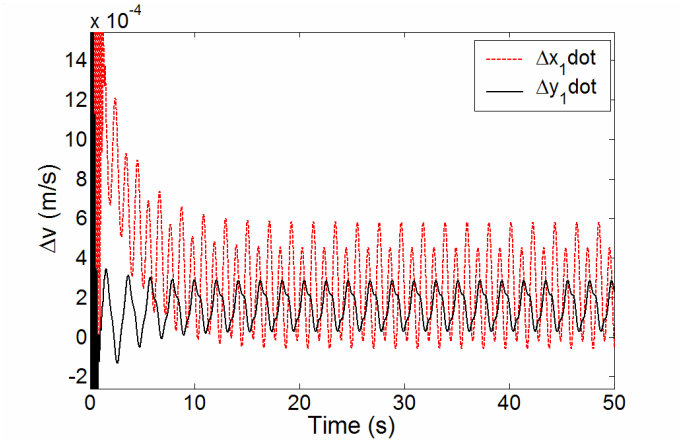

Fig. 7: Plot of the relative error in the translational velocities of the tail link of a three-link model

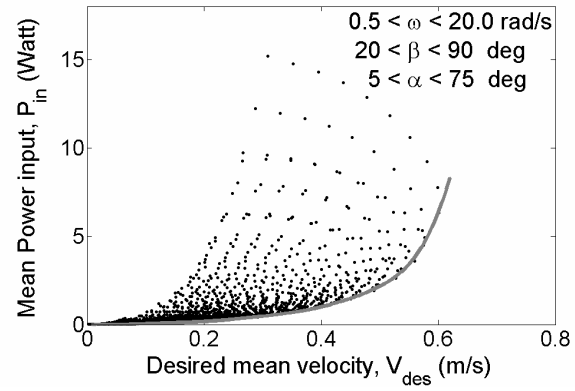

Fig. 8: Plot of P_{in} versus V_{des}

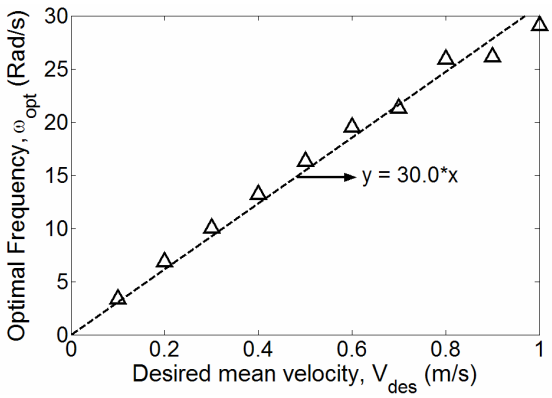

Fig. 9: Plot of ω_{opt} versus V_{des}

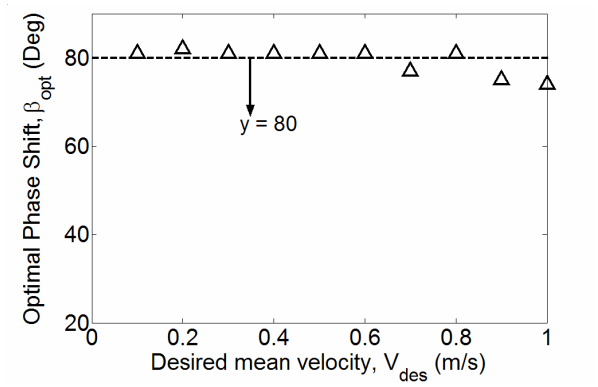

Fig. 10: Plot of β_{opt} versus V_{des}

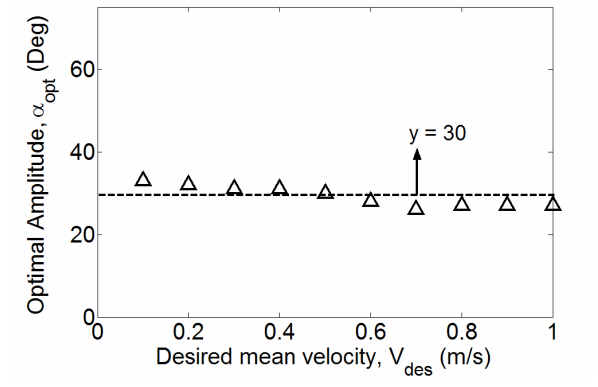

Fig. 11: Plot of α_{opt} versus V_{des}

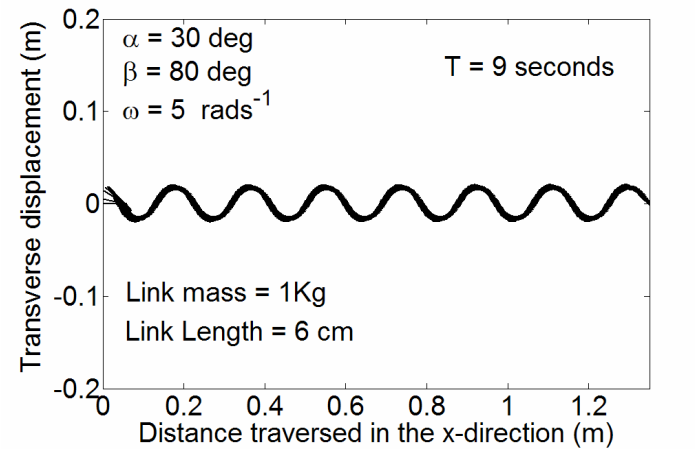

Fig. 12: Trace of the path followed by the snake robot at optimal parameter setting

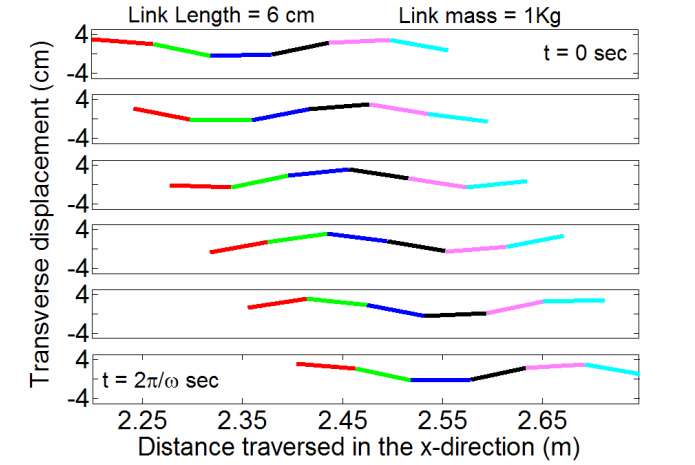

Fig. 13: Plot of the snake's position at six instances over one time period for $\alpha = 30$ deg, $\beta = 80$ deg, and $\omega = 3$ rads^{-1}

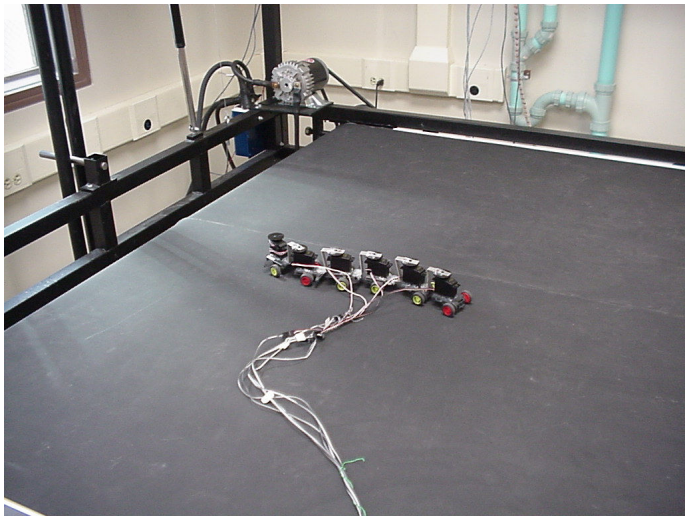

Fig. 14: Six-link robotic snake on treadmill

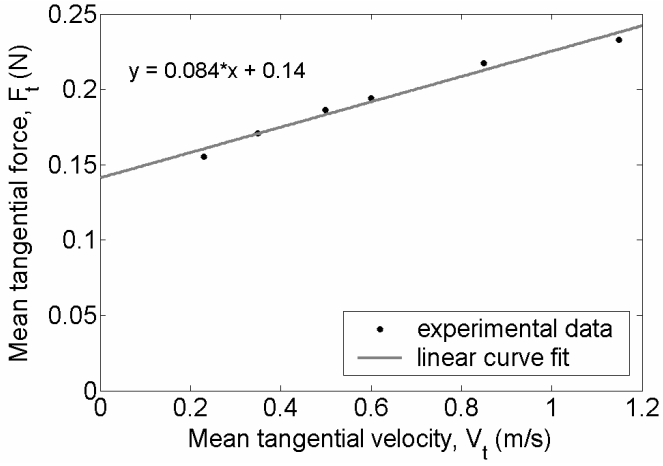

Fig. 15: Plot of mean tangential force, F_t, versus mean tangential velocity, V_t, to determine the tangential friction coefficient, C_t

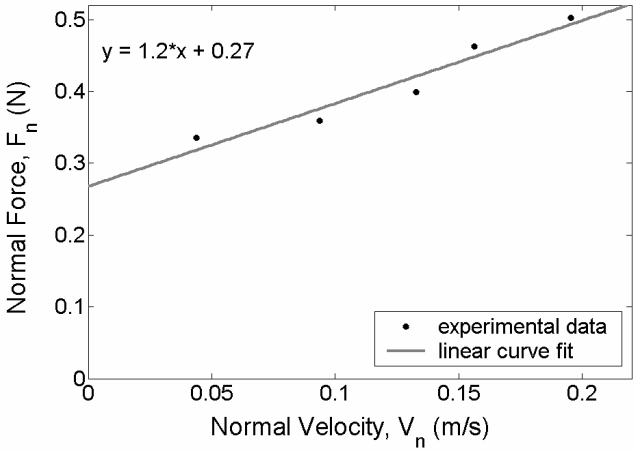

Fig. 16: Plot of the mean normal force, F_n, versus the mean normal velocity, V_n, to determine the normal friction coefficient, C_n

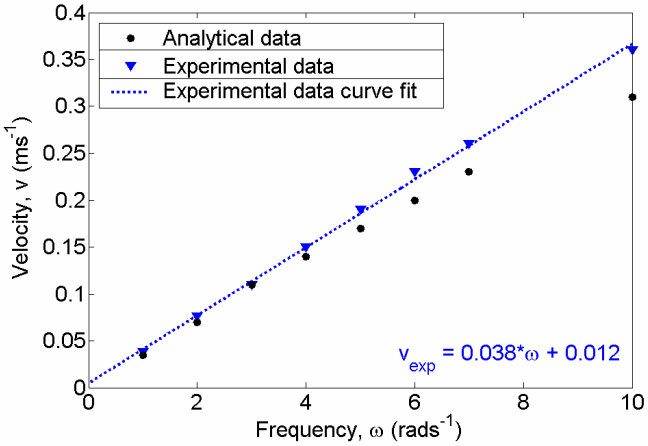

Fig. 17: Plot of the variation of analytical and experimental velocity as a function of frequency at $\alpha = 70$ deg and $\beta = 75$ deg corresponding to Bingham friction model